Research Square

Preprints are preliminary reports that have not undergone peer review.
They should not be considered conclusive, used to inform clinical practice,
or referenced by the media as validated information.

An anisotropic meandering model for atmospheric dispersion in low-wind-speed conditions

Julian Moises Sejje Suarez
Universidade Federal do Rio Grande
Antonio Goulart
antonio.goulart@furg.br
Universidade Federal do Rio Grande
Matheus Jatkoske Lazo
Universidade Federal do Rio Grande

Research Article

Keywords: Meandering, Low wind speed, Pollutant dispersion, Planetary boundary layer, Eddy diffusivity

Posted Date: September 23rd, 2026

DOI: https://doi.org/10.21203/rs.3.rs-10500136/v1

License: This work is licensed under a Creative Commons Attribution 4.0 International License.
Read Full License

Additional Declarations: No competing interests reported.

An anisotropic meandering model for atmospheric dispersion in low-wind-speed conditions

J. M. S. Suarez[1†], A. Goulart[1*†], M. J. Lazo[1†]

[1]Universidade Federal do Rio Grande, IMEF, Rio Grande, 96.201-900, RS, Brazil.

*Corresponding author(s). E-mail(s): antonio.goulart@furg.br;
Contributing authors: julian.sejje@furg.br; matheuslazo@furg.br;
†These authors contributed equally to this work.

Abstract

In this work, an analytical model for the dispersion of contaminants in low-wind-speed conditions is developed. The model combines the exact closed-form solution of the three-dimensional steady advection–diffusion equation with constant but distinct eddy diffusivities $\boldsymbol{K_x}$, $\boldsymbol{K_y}$ and $\boldsymbol{K_z}$, retaining the longitudinal diffusion term that cannot be neglected in weak winds, with an angular convolution of the resulting plume over a Gaussian distribution of wind directions, which represents the meandering of the horizontal wind. The horizontal eddy diffusivities are obtained from Taylor's statistical diffusion theory applied to the low-wind velocity spectrum of Mortarini and Anfossi, which explicitly contains the meandering peak, while the vertical eddy diffusivity is parameterised according to the stability regime of the planetary boundary layer. The model proposed is evaluated against the experimental data of the INEL experiment in a stable regime and the IIT Delhi experiment in a convective regime, and the statistical indices obtained are satisfactory. In addition, the model is compared with a semi-analytical multilayer solution (GIADMT) fed with the same horizontal diffusivities and the same meandering distribution, but retaining a height-dependent vertical eddy diffusivity. The comparison shows that the mathematically more complex multilayer model does not improve on the constant-coefficient closed form: in low wind the lateral spread is dominated by the meandering, and the ground-level concentration is controlled by the vertical diffusivity in the thin layer between source and receptor.

Keywords: Meandering, Low wind speed, Pollutant dispersion, Planetary boundary layer, Eddy diffusivity

1 Introduction

The dispersion of pollutants released in low-wind-speed conditions is one of the most critical and persistent problems in air quality modelling. When the mean wind speed falls below a threshold of about 1.5–2 $\mathrm{m\,s^{-1}}$, it is no longer possible to define a precise mean wind direction: the horizontal wind vector oscillates with periods of the order of half an hour or more, and these large low-frequency horizontal oscillations, known in the literature as meandering, come to dominate the transport of the contaminant, dispersing the plume over a rather wide angular sector [1, 28]. Low-wind episodes are far from exceptional, occurring for a substantial percentage of the time at many locations around the world [1], and they are often associated with the highest observed ground-level concentrations, since the weak advection allows the contaminant to accumulate near the source. At the same time, most operational dispersion models become unreliable as the wind speed approaches zero, so that their application is generally limited to wind speeds above about 2 $\mathrm{m\,s^{-1}}$ [1, 4].

Observational studies have delineated the phenomenology of meandering. Analysing two sonic anemometer datasets, one recorded in complex terrain and the other in a flat area, Anfossi et al. [1] found that meandering seems to exist under all meteorological conditions, regardless of stability, specific topographical features or season, and that it sets a lower limit for the variances of the horizontal wind components. Vickers and Mahrt [40], examining nine tower datasets over different surface types, concluded that the crosswind velocity variance associated with these mesoscale motions does not scale with the surface momentum flux nor with any other local parameter, so that its magnitude cannot be parameterised in terms of local variables. Mahrt [21] showed that, with weak large-scale flow, mesoscale motions on time scales up to one hour—internal gravity waves, microfront-like structures and horizontal modes—lead to meandering of the wind direction, which frequently takes the form of sudden wind shifts rather than of a regular oscillation. Maryon [22] processed long-period wind measurements to estimate the low-frequency crosswind variance required as input by dispersion models. Analysing sonic anemometer data measured in an urban canopy, Mortarini et al. [25, 26] observed the meandering also in a perturbed boundary layer and proposed that a low-wind meandering regime is identified by the joint conditions $\bar{u} < 1.5\,\mathrm{m\,s^{-1}}$ and loop parameter $m \geq 1$.

From the theoretical point of view, Oettl et al. [28] proposed that meandering is an inherent property of atmospheric flows in low-wind-speed conditions, requiring no particular trigger mechanism: solving the two-dimensional Reynolds-averaged Navier–Stokes equations with negligible Reynolds stresses, they showed that the oscillatory solution arises when the flow approaches geostrophic balance. Goulart et al. [11] extended this analysis to the three-dimensional equations and showed that the presence of turbulent forcing destroys the oscillatory behaviour, imposing a finite relaxation time and establishing a well-defined mean wind direction; meandering therefore prevails only when the turbulence is very weak.

The signature of meandering in one-point statistics is an oscillatory Eulerian autocorrelation function exhibiting large negative lobes, which the classical exponential form fails completely to describe. Anfossi et al. [1] showed that the function proposed by Frenkiel [10], containing the integral time scale T and a non-dimensional loop

parameter m that controls the meandering oscillation frequency, fits the experimental autocorrelation functions in low wind fairly well. Carvalho et al. [2] expressed the meandering parameters in terms of the characteristic velocity and length scales of the stable boundary layer, allowing their use in Lagrangian stochastic models. Moor et al. [23] proposed an alternative autocorrelation function and, from a large set of meandering events observed in the nocturnal boundary layer of the Amazon region, obtained the mean values $m_u = 4.8$ and $m_v = 5.1$ for the loop parameter and $T_* \approx 2200\,\mathrm{s}$ for the meandering period. In spectral space, Mortarini and Anfossi [27] proposed an empirical formula for the horizontal velocity spectrum in low wind that adds the meandering peak—the Fourier transform of the Frenkiel autocorrelation—to the classical inertial-subrange branch; this is the spectrum adopted in the present work to construct the horizontal eddy diffusivities.

Several modelling strategies have been employed to describe dispersion in low wind. In the Gaussian framework, Cirillo and Poli [4] compared semiempirical formulations against tracer data under stable, light-wind conditions and showed that the explicit consideration of diffusion along the mean wind direction, neglected in the standard plume model, significantly improves the results; Hanna [17] showed that at short distances the angular width of the time-averaged plume equals the standard deviation of the wind direction fluctuations, and that the lateral velocity fluctuation maintains a floor of about $0.5\,\mathrm{m\,s^{-1}}$ even as the wind speed approaches zero. In the Lagrangian framework, Carvalho et al. [2, 3] solved the Langevin equation by Picard's iterative method with the Frenkiel autocorrelation for the horizontal components, and Stefanello et al. [37] derived an analytical Lagrangian model for meandering conditions from the linearisation of the Langevin equation. In the Eulerian framework, Sharan et al. [34, 35] developed models for low wind with eddy diffusivities expressed as linear functions of the downwind distance, and Moreira et al. [24] solved the two-dimensional steady advection–diffusion equation, retaining the longitudinal diffusion, by the Laplace transform technique. In a recent work, Goulart et al. [12] evaluated eddy diffusivities derived from turbulence spectra in classical and fractional Eulerian dispersion models.

Two ingredients are, however, rarely combined in analytical Eulerian models. First, the longitudinal diffusion, which cannot be neglected at the small Péclet numbers typical of weak winds, is usually either dropped or retained only in two-dimensional solutions. Second, the meandering is often absorbed into a single enhanced effective lateral diffusivity, a procedure that reproduces the overall plume width but distorts the shape of the angular distribution of concentration. In this work we develop a model that treats these two ingredients separately and analytically. The diffusive core is the exact closed-form solution of the three-dimensional steady advection–diffusion equation with constant but distinct (anisotropic) eddy diffusivities K_x, K_y, K_z, retaining the longitudinal diffusion term; the meandering is represented explicitly by an angular convolution of this plume over a Gaussian distribution of wind directions. The horizontal eddy diffusivities are derived from Taylor's statistical diffusion theory applied to the low-wind spectrum of Mortarini and Anfossi [27], and the vertical eddy diffusivity is parameterised according to the stability regime [8, 15]. The model is validated against the low-wind tracer experiments of INEL [2, 32] in a stable boundary

layer and of IIT Delhi [34, 35] in a convective boundary layer. Furthermore, to isolate the role of the vertical diffusivity treatment, the model is compared with the semi-analytical multilayer GIADMT solution [5], fed with the same horizontal diffusivities and the same meandering distribution but retaining the full height-dependent vertical eddy diffusivity profile.

The convolution is the mathematical device that couples the meandering to the diffusive core of the model: the time-averaged concentration is written as the superposition of instantaneous plumes weighted by the probability density function of a slowly varying random variable—here, the wind direction. Although convolution techniques are not of widespread use in operational dispersion models for the planetary boundary layer, the idea that underlies them—when a fast, small-scale process is statistically independent of a slow, large-scale random displacement, the observed mean field is exactly the convolution of the kernel generated by the former with the probability density function of the latter—is well established in the description of turbulent transport. It is the foundation of the classical fluctuating plume framework, in which the probability density function of the concentration at a fixed point is the convolution of the density in the frame attached to the instantaneous plume centroid with the density of the centroid position [33]; Yee and Wilson [41] formalised this construction by expressing the absolute concentration density as a Weierstrass transform—a special case of the convolution transform, whose rigorous mathematical theory goes back to Hirschman and Widder [18]—of the relative-frame density, and Luhar et al. [20] used the same splitting into meander and relative dispersion to model concentration statistics in the convective boundary layer. Analogous constructions arise, beyond dispersion modelling, whenever a coherent structure wanders under the action of scales larger than itself: the long-term intensity profile of a laser beam propagating in turbulent air results from the superposition of the short-term diffractive profile onto the statistics of the beam wandering [13]; in radiation physics, the measured image or dose profile is the Gaussian convolution of an ideal source function blurred by scattering [38]; and dynamic wake meandering models for wind turbines treat the wake velocity deficit as a passive kernel advected by the low-pass-filtered large-scale atmospheric turbulence [14]. Even formulations that do not employ the term convolution share the same structure: the low-wind meander algorithm of AERMOD interpolates the horizontal concentration distribution between a plume component and a uniform angular component, a superposition weighted by the wind-direction statistics [39], and the analytical low-wind solutions of Sharan et al. [35] can be obtained by integrating the instantaneous puff solution over time, which is again a convolution of an elementary kernel. The angular convolution adopted in this work (Sect. 2) is the steady-state Eulerian counterpart of these constructions: the exact anisotropic plume plays the role of the invariant kernel and the Gaussian distribution of wind directions plays the role of the meandering statistics, so that the meandering enters the model as an explicit, physically transparent degree of freedom.

The paper is organized in the following way: In Sect. 2, the dispersion model is developed. In Sect. 3, the parameterization of turbulence in the planetary boundary layer is presented. A comparison of the model with experimental data and with the GIADMT solution is done in Sect. 4. Finally, Sect. 5 presents the conclusions.

2 Model development

The model is built from a purely diffusive core, the analytical solution of the three-dimensional advection–diffusion equation, to which an angular layer representing the meandering is coupled. The flow is assumed stationary and horizontally homogeneous over the averaging period (of the order of one hour), the source is continuous and the contaminant is passive and non-reactive. This section develops each step.

2.1 The three-dimensional advection–diffusion equation

Consider a continuous point source of strength Q located at $\mathbf{x}_0 = (0, 0, H_s)$ in a horizontally homogeneous mean flow $\mathbf{u} = (U, 0, 0)$, with constant turbulent eddy diffusivities K_x, K_y, K_z and no chemical decay. The steady advection–diffusion equation is

$$U\,\frac{\partial C}{\partial x} = K_x\frac{\partial^2 C}{\partial x^2} + K_y\frac{\partial^2 C}{\partial y^2} + K_z\frac{\partial^2 C}{\partial z^2} + Q\,\delta(x)\,\delta(y)\,\delta(z - H_s), \tag{1}$$

subject to total reflection at the ground, $\partial_z C|_{z=0} = 0$, and $C \to 0$ as $|x|, |y|, z \to \infty$. Retaining the longitudinal diffusion term $K_x\,\partial_x^2 C$—frequently dropped in classical Gaussian models—is essential in weak wind, where the Péclet number $\mathrm{Pe} = Ux/K_x$ is no longer large and the along-wind diffusion contributes materially to the transport [4, 24].

The constant eddy diffusivities K_x, K_y and K_z are prescribed by the turbulence parameterisation of Section 3: the horizontal diffusivities follow from Taylor's statistical diffusion theory applied to the low-wind velocity spectrum, while the vertical diffusivity is obtained by evaluating the height-dependent parameterisation appropriate to the stability regime at the height of the plume centreline (Section 3.2). The use of constant eddy diffusivities is consistent with the ground-level sources and receptors considered here, for which the plume remains confined to a shallow layer, and it is precisely this choice that will be tested against a height-dependent formulation in Section 4.3.

2.2 Coordinate isotropisation and the modified Helmholtz equation

Introducing the isotropised coordinates $\xi = x/\sqrt{K_x}$, $\eta = y/\sqrt{K_y}$, $\zeta = (z - H_s)/\sqrt{K_z}$, the anisotropic diffusion operator becomes the isotropic Laplacian $\Delta_{(\xi,\eta,\zeta)}$, and the scaling property of the Dirac delta gives $\delta(x)\delta(y)\delta(z-H_s) = \delta(\xi)\delta(\eta)\delta(\zeta)/\sqrt{K_xK_yK_z}$. Equation (1) reduces to

$$\tilde{U}\,\partial_\xi C = \Delta C + \tilde{Q}\,\delta(\xi)\delta(\eta)\delta(\zeta), \qquad \tilde{U} = \frac{U}{\sqrt{K_x}}, \quad \tilde{Q} = \frac{Q}{\sqrt{K_xK_yK_z}}. \tag{2}$$

The advection is removed by the exponential substitution $C = e^{\tilde{\beta}\xi}\,w$ with $\tilde{\beta} = \tilde{U}/2$. The terms linear in $\partial_\xi w$ cancel and one obtains the modified Helmholtz equation with

a point source,

$$\left(\Delta - \tilde{\alpha}^2\right) w = -\tilde{Q}\,\delta(\xi)\delta(\eta)\delta(\zeta), \qquad \tilde{\alpha}^2 = \tilde{\beta}^2 = \frac{U^2}{4K_x}. \tag{3}$$

2.3 The Green function and ground reflection

The decaying three-dimensional fundamental solution of (3) is the Green function, $w(\tilde{\rho}) = (\tilde{Q}/4\pi)\, e^{-\tilde{\alpha}\tilde{\rho}}/\tilde{\rho}$, with $\tilde{\rho} = \sqrt{\xi^2 + \eta^2 + \zeta^2}$. The zero-flux ground condition is satisfied by the method of images, adding a mirror source at $z = -H_s$. Defining the isotropised distances to the real source and to the image,

$$\tilde{\rho}_{\pm} = \sqrt{\frac{x^2}{K_x} + \frac{y^2}{K_y} + \frac{(z \mp H_s)^2}{K_z}}, \tag{4}$$

and undoing the exponential transformation, the closed-form diffusive core of the model is the three-dimensional Helmholtz plume

$$C_{3D}(x, y, z) = \frac{Q}{4\pi\sqrt{K_x K_y K_z}}\, \exp\!\Big(\frac{Ux}{2K_x}\Big) \left[\frac{e^{-\tilde{\alpha}\tilde{\rho}_+}}{\tilde{\rho}_+} + \frac{e^{-\tilde{\alpha}\tilde{\rho}_-}}{\tilde{\rho}_-}\right], \tag{5}$$

with $\tilde{\alpha} = U/(2\sqrt{K_x})$. Equation (5) is exact—no Laplace inversion or infinite series is required—and yields the concentration directly at any receptor. For $K_x = K_y = K_z$ it reduces to the classical spherical Helmholtz solution with reflection, and in the limit of large Péclet number ($Ux/K_x \gg 1$) it recovers, downwind of the source, the classical Gaussian plume with $\sigma_y^2 = 2K_y x/U$ and $\sigma_z^2 = 2K_z x/U$, so that the solution is consistent with the standard model in the windy regime. Because the combined argument $Ux/(2K_x) - \tilde{\alpha}\tilde{\rho}_{\pm}$ is always ≤ 0, the arithmetic stays in $(0, 1]$, avoiding numerical overflow at the large Péclet numbers (Pe $\sim 10^4$) that occur far downwind.

2.4 Angular convolution: lateral meandering

Solution (5) describes a plume from a wind of fixed direction. To represent meandering, we assume that during the averaging period the wind vector points in a direction θ about the x axis, distributed according to a Gaussian probability density function (in the small-angle approximation $\theta \approx v/U$),

$$p(\theta) = \frac{1}{\sqrt{2\pi}\,\sigma_\theta}\, \exp\!\Big(-\frac{\theta^2}{2\sigma_\theta^2}\Big). \tag{6}$$

The mean observed concentration is the superposition (angular convolution) of the instantaneous plumes, each rotated by θ:

$$C_{3D}^{\mathrm{FO}}(x, y, z) = \int_{-\theta_{\max}}^{\theta_{\max}} p(\theta)\, C_{3D}\big(x', y', z\big)\, d\theta, \qquad \begin{aligned} x' &= x\cos\theta + y\sin\theta, \\ y' &= -x\sin\theta + y\cos\theta, \end{aligned} \tag{7}$$

with $\theta_{\max} = \min(4\sigma_\theta,\, 0.99\,\pi/2)$, evaluated by Simpson quadrature. The superscript FO refers to the Frenkiel–Oettl description of the meandering [10, 28] that underlies the angular distribution; Eqs. (5)–(7) constitute the proposed model in this work. The angular width σ_θ is the only new ingredient of this layer (Section 3.3). As $\sigma_\theta \to 0$ the density (6) collapses to $\delta(\theta)$ and (7) returns (5) exactly, so that the model reduces continuously to the purely diffusive plume when the meandering vanishes. The Gaussian form of $p(\theta)$ is consistent with the observation [21] that meandering often manifests as wind shifts rather than as a strict oscillation, so that the relevant quantity for the time-averaged plume is the angular distribution of the wind direction rather than its detailed time history.

3 Turbulence parameterization in the planetary boundary layer

3.1 Horizontal eddy diffusivities

To obtain the horizontal eddy diffusivities, we will consider Taylor's statistical theory applied to the low-wind turbulence spectrum. In the asymptotic ($t \to \infty$) limit, the Batchelor eddy diffusivity can be written as [7, 12],

$$K_\gamma = \tfrac{a}{4}\, U\, F_j(0)\, \sigma_j \tag{8}$$

where $F_j(0)$ is the value at zero frequency of the normalised spectrum, U is the mean transport wind, $a = \sqrt{\pi}/4$ and $j = u, v$ for $\gamma = x, y$, respectively.
To account for the weak wind regime, we will use the model of Mortarini and Anfossi for the horizontal components of the spectrum [27], which sums the meandering peak (the Fourier transform of the oscillating Frenkiel autocorrelation) to a Kaimal inertial branch,

$$F_j(n) = \alpha_j \frac{4\{T + 4(1+m^2)\, n^2\pi^2 T^3\}}{1 + 8(1-m^2)\pi^2 n^2 T^2 + 16(1+m^2)^2\pi^4 n^4 T^4} + \frac{(\tilde{n}-1)^2}{1+\lambda\tilde{n}+\tilde{n}^2}\, \frac{0.164\, n/n_0}{1 + 0.164\,(n/n_0)^{5/3}}, \tag{9}$$

with $\tilde{n} = n/n_{\max}$, $\lambda = 40$, $T \equiv T_E$ the Eulerian integral time scale, peak frequency $n_{\max} = \sqrt{p^2+q^2}/(2\pi)$, where m is the loop parameter, which controls the meandering oscillation frequency, and $p = 1/[T(1+m^2)]$ and $q = m/[T(1+m^2)]$ are expressed in terms of (T, m). The coefficient α_j is the normalisation coefficient that guarantees $\int_0^\infty F_j(n)\, dn = 1$, and is evaluated numerically for each case [27]. Evaluating at $n = 0$ the second (inertial) term vanishes and $F_j(0) = 4\,\alpha_j\, T_E$. Substituting into (8), we obtain the following expressions for the horizontal eddy diffusivities,

$$K_x = \frac{\sqrt{\pi}}{4}\, U\, \alpha_u\, T_{E,u}\, \sigma_u, \qquad K_y = \frac{\sqrt{\pi}}{4}\, U\, \alpha_v\, T_{E,v}\, \sigma_v. \tag{10}$$

The parameters $(\sigma_j, T_{E,j}, m_j)$ will be described in Section 4 for each experiment; Eq. (10) then yields directly the constant values of K_x and K_y used in Eq. (5).

3.2 Vertical diffusivity by stability regime

The vertical eddy diffusivity is calculated according to the stability regime.

Stable boundary layer.

For $L > 0$ we use the eddy diffusivity proposed by Degrazia et al. [8],

$$K_z^{\mathrm{SBL}}(z) = \frac{0.4\, u_*\, z\,(1 - z/h)}{1 + 3.7\,\dfrac{z}{\Lambda}}, \tag{11}$$

where u_* is the friction velocity and $\Lambda = L(1 - z/h)^{5/4}$ is the local Monin–Obukhov length, L being the Obukhov length.

Convective boundary layer, surface sources.

For $L < 0$ and low sources the vertical diffusivity is built from Taylor's asymptotic statistical-theory relation $K_z = \sigma_w^2\, T_{Lw}$, using the convective surface-layer similarity expressions of Hanna [15] for the vertical velocity standard deviation, $\sigma_w = 1.3\, u_*\,(1 - 3z/L)^{1/3}$, and for the vertical Lagrangian time scale his unstable surface-layer form $T_{Lw} = 0.1\,(z/\sigma_w)\,[\,0.55 + 0.38\,(z - z_0)/|L|\,]^{-1}$. Their product gives the surface-layer form

$$K_z^{\mathrm{CBL}}(z) = \frac{0.13\, u_*\, z\,\left(1 - 3z/L\right)^{1/3}}{0.55 + 0.38\,(z - z_0)/|L|}. \tag{12}$$

In both stability regimes the constant K_z used in Eq. (5) is obtained by evaluating the corresponding profile, Eq. (11) or (12), at the height of the plume centreline over the sampling arcs. For a ground-reflected plume the mean height of the contaminant is $\bar{z} = \sqrt{2/\pi}\,\sigma_z$, with $\sigma_z = \sqrt{2K_z x/U}$, so that $\bar{z}$ and K_z are determined self-consistently by a fixed-point iteration that converges in a few steps; the resulting $\bar{z}$ is averaged over the arc distances of each experiment. In the stable INEL experiment of Section 4.1 this criterion gives $\bar{z} \approx 0.9$–$2.5\,\mathrm{m}$, depending on the experiment. In the convective case the same criterion is essential rather than merely convenient: the mixed layer ($z_i \sim 10^3\,\mathrm{m}$) is three orders of magnitude deeper than the shallow layer actually occupied by a near-surface plume at short range, so that a vertical average over z_i would be dominated by the vigorous mixing of the bulk of the convective boundary layer, which the plume never samples, and would grossly overestimate the vertical spread. For the IIT Delhi geometry of Section 4.2, $\sigma_z \approx 4$–$7\,\mathrm{m}$ at $x = 50$–$100\,\mathrm{m}$, corresponding to $\bar{z} \approx 3$–$5\,\mathrm{m}$; Eq. (12) is evaluated at $z = 3\,\mathrm{m}$.

3.3 Angular width σ_θ and lateral variance σ_v

Following Cirillo and Poli [4], the second moment of $U \sin\theta$ with $\theta \sim \mathcal{N}(0, \sigma_\theta^2)$ gives the exact relation $\sigma_v^2 = \frac{\bar{U}^2}{2}(1 - e^{-2\sigma_\theta^2})$, which in the small-angle limit reduces to $\sigma_\theta \approx \sigma_v/\bar{U}$ (the difference is less than 5% up to $\sigma_\theta \approx 50^\circ$ [4]). The lateral variance is

parameterised in two stability ranges with the Hanna [17] low-wind floor in both:

$$\sigma_v = \begin{cases} \max\Big(u_*\big[2.0 + 4.0\,(z/L)^{0.6}\big],\, 0.5\,\mathrm{m\,s^{-1}}\Big), & L > 0 \text{ (SBL, [29])}, \\ \max\Big(u_*\big(12 + 0.5\,z_i/|L|\big)^{1/3},\, 0.5\,\mathrm{m\,s^{-1}}\Big), & L < 0 \text{ (CBL, [30])}, \end{cases} \tag{13}$$

and then $\sigma_\theta = \sigma_v/U$. The floor guarantees a minimum meandering in very weak wind, in line with the empirical lower bound on the horizontal variance reported by Anfossi et al. [1] and Vickers and Mahrt [40]. As discussed in Section 1, the mesoscale part of σ_v is not parameterisable locally [21, 40]; Eq. (13) captures the correct mean magnitude but not the experiment-to-experiment variability, which affects the correlation coefficient *Cor* but not the other indices.

3.4 Wind profile

The wind velocity is taken at a height representative of the vertical centroid of the plume. In the stable boundary layer a power-law profile anchored at the measurement height z_1 [31],

$$u(z) = u(z_1)\Big(\frac{z}{z_1}\Big)^p, \tag{14}$$

where $u(z)$ and $u(z_1)$ are the mean wind velocity at the heights z and z_1, respectively, while p is an exponent that is related to the intensity of turbulence [19].
In the convective boundary layer the transport wind is taken directly as the measured mean wind speed of each experiment (Table 4).

4 Results and discussion

The performance of the model proposed in this work, expressed by Eqs. (5)–(7) with the eddy diffusivities given by Eqs. (10), (11) and (12), was evaluated against the experimental ground-level concentrations of two low-wind field experiments with near-surface sources: the INEL experiment in a stable boundary layer, for which both the peak concentration and the full angular distribution along the sampling arcs are examined, and the IIT Delhi experiment in a convective boundary layer.
To compare the simulated and observed concentrations, the statistical indices described in Hanna [16] are used:

$$\begin{aligned} \textit{NMSE}\ \text{(normalized mean-square error)} &= \frac{\overline{(c_o - c_p)^2}}{\overline{c_o}\;\overline{c_p}}, \\ \textit{Cor}\ \text{(correlation coefficient)} &= \frac{\overline{(c_o - \overline{c_o})(c_p - \overline{c_p})}}{\sigma_o\,\sigma_p}, \\ \textit{FB}\ \text{(fractional bias)} &= \frac{\overline{c_o} - \overline{c_p}}{0.5(\overline{c_o} + \overline{c_p})}, \\ \textit{FS}\ \text{(fractional standard deviations)} &= \frac{\sigma_o - \sigma_p}{0.5(\sigma_o + \sigma_p)}, \end{aligned}$$

where c_p is the computed concentration, c_o the observed concentration, σ_p and σ_o the computed and observed standard deviations, and the overbar denotes an averaged value. The index *FA2* is the fraction of data for which $0.5 \leq c_p/c_o \leq 2$. The best results are indicated by values nearest to 0 in *NMSE*, *FS* and *FB*, and nearest to 1 in *Cor* and *FA2*. The acceptance criteria are $|FB| < 0.3$, $|FS| < 0.5$, $FA2 \geq 0.5$ and $NMSE < 0.5$.

4.1 INEL experiment

The Idaho National Engineering Laboratory (INEL) site is flat and rural. The experiment was conducted during stable low-wind conditions [32]. Because of wind direction variability, a full 360° sampling grid was implemented. Arcs were laid out at radii of 100, 200 and 400 m from the emission point. Samplers were placed at intervals of 6° on each arc for a total of 180 sampling positions. The receptor height was 0.76 m. The tracer SF_6 was released at a height of 1.5 m. The micrometeorological data are given in Table 1. For the INEL experiment we consider $p = 0.6$ in the wind velocity profile given by Eq. (14).

Meandering parameters.

The horizontal eddy diffusivities K_x, K_y (Eq. (10)) are supplied, experiment by experiment, with the meandering statistics described below, each obtained as a vertical average over the boundary-layer height h. The horizontal velocity standard deviations follow the stable-boundary-layer local-scaling forms $\sigma_u(z) = 2.0\,u_*\,(1 - z/h)^{3/4}$ and $\sigma_v(z) = 1.44\,u_*\,(1 - z/h)^{3/4}$ [8], collapsed to a single value through the vertical root mean square $\sigma_j = \left[h^{-1}\int_0^h \sigma_j^2(z)\,dz\right]^{1/2}$. The Eulerian integral time scales use the relation [8, 23],

$$T_j(z) = \frac{z}{\sqrt{c_j}}\,\frac{0.50}{u_*\,\phi_\varepsilon^{1/3}\,(1 + 3.7\,z/\Lambda)^{2/3}}, \qquad c_u = 0.27,\ c_v = 0.36, \tag{15}$$

with $\phi_\varepsilon = 1.1\,(1 + 3.7\,z/\Lambda)$ and $\Lambda = L(1 - z/h)^{5/4}$ [23], again vertically averaged to give $T_{E,u}, T_{E,v}$; the loop parameters are $m_u = 4.8$ and $m_v = 5.1$ [23]. The resulting values are listed in Table 2; the three experiments without a spectral fit (5, 7, 8) revert to the Hanna low-wind fallback ($\sigma_u = 2.5\,u_*$, $\sigma_v = 2.0\,u_*$, $T_E = 6\,\mathrm{s}$, $m = 4.8$) [15]. The angular width is calculated by $\sigma_\theta = \sigma_v/U$, using the σ_v calculated by Eq. (13) [29]. The constant vertical diffusivity is Eq. (11) evaluated at the height of the plume centreline ($\bar{z} \approx 0.9$–$2.5\,\mathrm{m}$), as described in Section 3.2.

Table 3 shows the results of the statistical indices used to evaluate the model performance for the INEL experiment, and Fig. 1 shows the corresponding scatter diagram. It is possible to see the good performance of the model, especially in the factor-of-two index ($FA2 = 0.87$), with all indices within the acceptance ranges. For comparison, Table 3 also reports the results of the model of Moreira et al. [24], which solves the two-dimensional steady-state advection–diffusion equation using the Laplace transform and adopts the height-dependent eddy diffusivity proposed by Degrazia and Moraes [6].

Table 1 Micrometeorological data for the INEL experiment (stable case). U is the transport wind from Eq. (14) evaluated at $z = 4\,\mathrm{m}$.

Exp.	h (m)	u_* ($\mathrm{m\,s^{-1}}$)	L (m)	U ($\mathrm{m\,s^{-1}}$)
4	13.40	0.047	2.40	1.2
5	16.38	0.053	3.14	0.9
7	10.64	0.040	1.77	0.9
8	8.09	0.033	1.22	0.8
9	8.09	0.033	1.22	0.8
10	26.40	0.073	5.93	1.7
11	37.91	0.093	9.60	1.9
12	13.40	0.047	2.40	1.1
13	22.88	0.067	4.90	1.6
14	22.88	0.067	4.90	1.5

Table 2 INEL meandering parameters feeding K_x, K_y (Eq. (10)). In all experiments $m_u = 4.8$, $m_v = 5.1$.

Exp.	σ_u ($\mathrm{m\,s^{-1}}$)	σ_v ($\mathrm{m\,s^{-1}}$)	$T_{E,u}$ (s)	$T_{E,v}$ (s)
4	0.059	0.043	4.62	4.00
9	0.042	0.030	3.42	2.97
10	0.092	0.067	7.12	6.16
11	0.118	0.085	8.87	7.68
12	0.059	0.043	4.62	4.00
13	0.085	0.061	6.45	5.59
14	0.085	0.061	6.45	5.59

Table 3 Statistical indices of the model given by Eqs. (7), (10) and (11) for the INEL experiment.

Model	Cor	NMSE	FS	FB	FA2
Eqs. (7), (10) and (11)	0.58	0.39	0.00	−0.17	0.87
Moreira et al. (2005) [24]	0.79	0.25	+0.08	+0.02	0.79

4.2 IIT Delhi experiment

Dispersion experiments under low-wind convective conditions were conducted by the Indian Institute of Technology (IIT Delhi) and described in Sharan et al. [34, 35]. The pollutant was released without buoyancy at a height of 1 m and the concentrations of SF_6 were observed near the ground level (0.5 m). The release rate of the SF_6 tracer varied from 30 to 50 $\mathrm{ml\,min^{-1}}$. The sampling period for each run was 30 min. Wind velocity and temperature measurements were obtained at four levels (2, 4, 15 and 30 m). In all the cases, the wind velocity was less than $2\,\mathrm{m\,s^{-1}}$. The samplers were

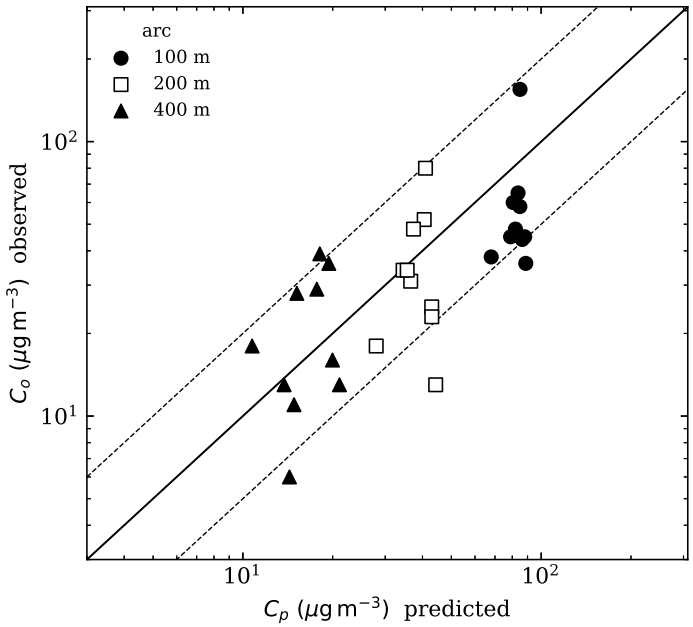


Fig. 1 Scatter diagram between predicted (C_p) and observed (C_o) ground-level concentration for the INEL experiment. Markers denote the sampling arcs. Solid line $C_o = C_p$; dashed lines $C_o = 2C_p$ and $C_o = C_p/2$.

located on arcs of 50 and 100 m radii. The micrometeorological data are given in Table 4.

Meandering parameters.

The horizontal eddy diffusivities K_x, K_y (Eq. (10)) use the Hanna [15] low-wind fall-back, identical for every experiment, $\sigma_u = 2.5\,u_*$, $\sigma_v = 2.0\,u_*$, $T_{E,u} = T_{E,v} = 6$ s and $m_u = m_v = 4.8$. The angular width is calculated by $\sigma_\theta = \sigma_v/U$, using the σ_v calculated by Eq. (13) [30]. The constant vertical diffusivity is Eq. (12) evaluated at $z = 3$ m, the mean height of the plume over the sampling arcs, as described in Section 3.2.

Table 5 shows the results of the statistical indices for the IIT Delhi experiment, and Fig. 2 the corresponding scatter diagram; for comparison, the table also reports the results of two models from the literature applied to the same experiment. The model proposed by Moreira et al. [24] solves the steady-state two-dimensional advection–diffusion equation using the Laplace transform and adopts the turbulent diffusivity, dependent on height and on the downwind distance from the source, proposed by Degrazia et al. [9]. The model proposed by Sharan et al. [36] employs the analytical solution of the steady-state three-dimensional advection–diffusion equation with eddy diffusivities parameterised as linear functions of the downwind distance [35], with the coefficients expressed in terms of the friction velocity. All the indices of the model proposed in this work satisfy the acceptance criteria, showing that the model also performs well in the convective regime; it attains the lowest NMSE and the highest

Table 4 Micrometeorological data for the IIT Delhi experiment.

Exp.	z_i (m)	u_* (m s^{-1})	L (m)	U (m s^{-1})	w_* (m s^{-1})
1	1570	0.39	−17.5	1.36	2.37
2	1240	0.21	−2.5	0.74	2.26
6	1070	0.40	−20.0	1.40	2.04
7	1240	0.44	−22.0	1.54	2.28
8	943	0.26	−32.0	0.89	1.09
11	1070	0.31	−13.0	1.07	1.83
12	1325	0.45	−24.0	1.55	2.32
13	1070	0.16	−2.0	1.08	1.72

FA2 of the three models. The model of Sharan et al., although reaching a somewhat higher correlation, underestimates the observed concentrations, with a fractional bias ($FB = +0.45$) that exceeds the acceptance limit.

Table 5 Statistical indices of the model given by Eqs. (7), (10) and (12) for the IIT Delhi experiment.

Model	Cor	NMSE	FS	FB	FA2
Eqs. (7), (10) and (12)	0.85	0.16	−0.15	−0.13	0.88
Moreira et al. (2005) [24]	0.76	0.35	−0.33	−0.01	0.81
Sharan et al. (2002) [36]	0.91	0.37	+0.40	+0.45	0.75

4.3 Comparison with a height-dependent multilayer model (GIADMT)

A natural question is whether a model that solves the three-dimensional advection–diffusion equation with height-dependent coefficients would outperform the constant-coefficient closed form given by Eq. (5). To answer this question we use the semi-analytical GIADMT (Generalized Integral Advection–Diffusion Multilayer Technique) [5], which solves Eq. (1) with vertically variable coefficients $K_x(z)$, $K_y(z)$, $K_z(z)$ and $u(z)$ by combining a generalised integral-transform expansion in the crosswind coordinate, a multilayer discretisation in z in which the coefficients are held constant within each sublayer, and a Laplace transform in the longitudinal coordinate, inverted numerically. With constant coefficients the scheme reproduces the analytical solution (5) to better than 1%.

To make the comparison meaningful, the GIADMT is fed with the same horizontal eddy diffusivities K_x, K_y (Eq. (10)) and is closed by the same Gaussian angular convolution (Eqs. (6)–(7)) as the model proposed in this work, so that the meandering is represented identically in the two models. The essential difference lies in the treatment of the vertical diffusion: the GIADMT retains a full height-dependent stable-boundary-layer profile $K_z(z)$, derived from the turbulent velocity spectrum [12],

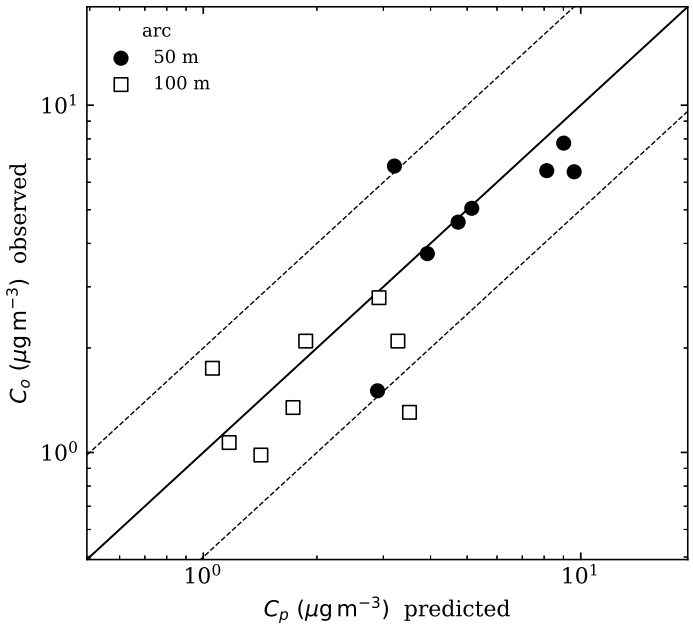


Fig. 2 Scatter diagram between predicted (C_p) and observed (C_o) ground-level concentration for the IIT Delhi experiment. Markers denote the sampling arcs. Solid line $C_o = C_p$; dashed lines $C_o = 2C_p$ and $C_o = C_p/2$.

whereas the model proposed in this work uses the constant K_z of Section 3.2, evaluated at the height of the plume centreline. The angular convolution of the multilayer plume was verified against its narrow-kernel limit at $x = 100\,\mathrm{m}$ for three representative wind regimes (Exps. 9, 4 and 11), with agreement better than 9% for the ground-level peak; the small residual deficit of the strongest-wind case reflects only the slight overestimation of the narrow-kernel limit when the width of the diffusive core is not negligible with respect to the arc distance. The comparison therefore probes chiefly the treatment of the vertical diffusion, not the meandering. Two observables of the INEL experiment are examined: the ground-level peak concentration (Section 4.3.1) and the full angular distribution of the concentration along the sampling arcs (Section 4.3.2).

4.3.1 Ground-level peak concentration

Table 6 presents the statistical indices of the two models for the INEL peak concentrations ($N = 30$), together with the K-diffusion reference model of Moreira et al. [24]. The GIADMT, fed with the height-dependent profile $K_z(z)$, systematically overestimates the observed peak and fails the acceptance criteria, whereas the model proposed in this work, with the same meandering distribution but the constant K_z, remains well calibrated. Figure 3 illustrates the difference: the GIADMT points (panel a) lie mostly on the overestimation side of the $C_o = C_p$ line, while the constant-coefficient model (panel b) is well centred.

The origin of the discrepancy is the value of the vertical diffusivity in the shallow layer occupied by the plume, which at these distances remains within the lowest few metres. The height-dependent profile vanishes at the ground, so in the thin layer containing source and receptor ($z \approx 0.76$–$1.5\,\mathrm{m}$) the multilayer solution operates with a K_z a factor of 5–10 smaller than the constant K_z used by the model proposed in this work; since in weak wind the near-field concentration scales essentially as $(K_x K_y K_z)^{-1/2}$ (Eq. (5)), this deficit of vertical dilution keeps the contaminant close to the ground and inflates the predicted concentration. The ground-level peak is therefore extremely sensitive to the value of K_z in the source–receptor layer. Solving the three-dimensional equation with height-dependent diffusivities—a mathematically far more complex procedure—does not improve on the closed-form constant-coefficient solution: in weak wind the lateral spread is dominated by the meandering, which is captured equally well by the angular convolution in both models, and the peak is controlled by that lateral width and by the source-layer K_z, whose value at the height of the plume centreline proves better calibrated than the local values of the profile.

Table 6 INEL peak concentrations ($N = 30$): GIADMT with the height-dependent $K_z(z)$ profile vs the model proposed in this work (constant K_z at the plume centreline height), both with the same horizontal diffusivities and the same $p(\theta)$, and the K-diffusion reference. Acceptable: $|FB| < 0.3$, $|FS| < 0.5$, FA2 ≥ 0.5, NMSE < 0.5.

Model	Cor	NMSE	FS	FB	FA2
GIADMT, $K_z(z)$ profile	0.59	1.80	−0.71	−0.98	0.20
Eqs. (7), (10) and (11) (constant K_z)	0.58	0.39	0.00	−0.17	0.87
K-diffusion – Moreira et al. (2005) [24]	0.79	0.25	+0.08	+0.02	0.79

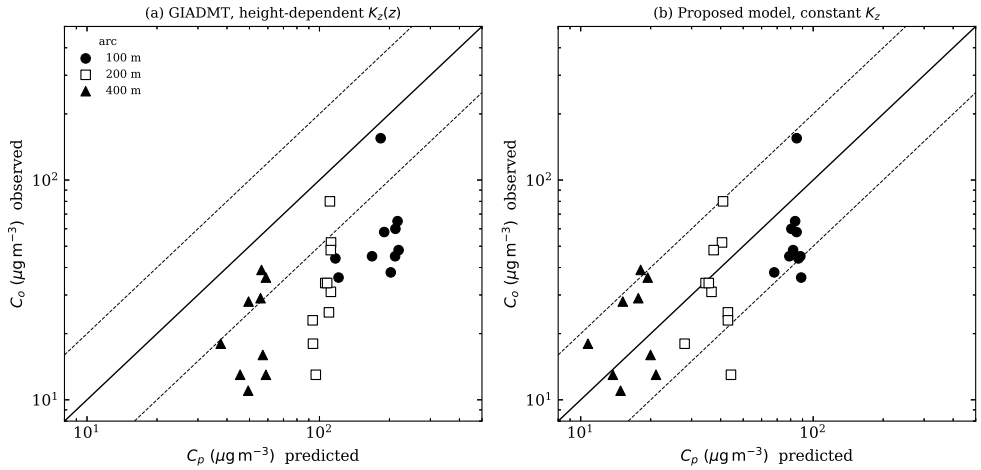


Fig. 3 INEL ($N = 30$): predicted vs observed peak concentration. (a) GIADMT with the height-dependent $K_z(z)$ profile; (b) proposed model with constant K_z. Solid line $C_o = C_p$; dashed lines, FA2 band.

4.3.2 Angular distribution of the concentration along the arcs

A more demanding test at the same site is the angular distribution of the normalised concentration $\chi U/Q$ along each sampling arc, which resolves not only the peak but also the lateral tails—the very signature of meandering. For each low-wind experiment, $\chi U/Q$ is measured at 9–27 azimuths across the arcs at 100, 200 and 400 m; the seven experiments for which the meandering parameters could be determined from the spectral fit (4, 9, 10, 11, 12, 13, 14; Table 2) are used, giving $N = 339$ points. Because the diffusive core is written in a wind-aligned frame, each measurement azimuth θ is first projected onto the wind direction θ_w through $\Delta = \theta - \theta_w$, $x = r\cos\Delta$, $y = r\sin\Delta$, before the angular convolution (7) is applied.

Table 7 compares, experiment by experiment, the root-mean-square error of the GIADMT, evaluated on the same arcs with the same meandering $p(\theta)$, and of the model proposed in this work. The latter reduces the RMSE in all seven experiments, by factors of 1.9 to 4.2 (mean $\approx$ 3.4). The gain is remarkably uniform across the experiments: since the two models share the same angular kernel, the improvement does not depend on the meandering intensity, but stems entirely from the treatment of the vertical diffusion.

Table 7 INEL — angular distribution $\chi U/Q$ along the arcs. RMSE (on the $\chi U/Q$ scale, $\times 10^{-3}$) of the GIADMT (height-dependent $K_z(z)$) and of the model proposed in this work (constant K_z at the plume centreline height), both sharing the same K_x, K_y and the same $p(\theta)$. K_z in $10^{-3}\,\mathrm{m^2/s}$; σ_θ in degrees; $U = U_{4\mathrm{m}}$.

Exp	u_* (m/s)	U (m/s)	K_z	σ_θ (°)	$\mathrm{RMSE}_{\mathrm{GIADMT}}$	$\mathrm{RMSE}_{\mathrm{3D}}$
4	0.047	1.20	6.7	23.9	2.34	**0.96**
9	0.033	0.80	2.5	35.8	1.78	**0.95**
10	0.073	1.70	22.4	16.9	3.27	**1.02**
11	0.093	1.90	42.2	15.1	2.87	**0.73**
12	0.047	1.10	6.7	26.0	1.77	**0.44**
13	0.067	1.60	17.6	17.9	3.14	**0.76**
14	0.067	1.50	17.7	19.1	3.19	**0.77**

Table 8 collects the aggregated statistical indices over the $N = 339$ points for the two models. Three features stand out. First, the two models share essentially the same correlation ($Cor \approx 0.67$): the angular ordering of the points is set by the meandering kernel $p(\theta)$, which is common to both, so that the differences lie in magnitude and shape, not in ranking. Second, the GIADMT strongly overestimates the concentration along the arcs ($FB = -1.15$, FA2 = 0.12), for the same reason identified in Section 4.3.1: the height-dependent $K_z(z)$ profile supplies too little vertical diffusivity in the shallow layer occupied by the plume, keeping the contaminant close to the ground along the whole arc. Replacing that profile by the constant K_z evaluated at the plume centreline height lowers the aggregated NMSE from 5.15 to 1.16 and raises FA2 from 0.12 to 0.40 (Fig. 4). Third, even the model proposed in this work does

not meet the acceptance criteria on this observable ($NMSE = 1.16$, $FB = -0.34$, FA2 $= 0.40$). It is worth stating why the arc test is so much more demanding than the peak test of Section 4.3.1: the angular distribution weighs every azimuth equally, including the far lateral tails, where the measured $\chi U/Q$ falls two to three orders of magnitude below the peak and where both the wind-direction record and the sampler detection limit are least reliable, so that relative errors that are invisible at the peak dominate a large fraction of the $N = 339$ points.

Table 8 INEL arcs ($N = 339$): aggregated statistical indices for the GIADMT (height-dependent $K_z(z)$) and the model proposed in this work (constant K_z at the plume centreline height), both sharing the same K_x, K_y and the same $p(\theta)$. Acceptable: $|FB| < 0.3$, $|FS| < 0.5$, FA2 ≥ 0.5, NMSE < 0.5.

Model	Cor	NMSE	FS	FB	FA2
GIADMT, $K_z(z)$ profile	0.67	5.15	−1.07	−1.15	0.12
Eqs. (7), (10) and (11) (constant K_z)	0.68	**1.16**	**−0.27**	**−0.34**	**0.40**

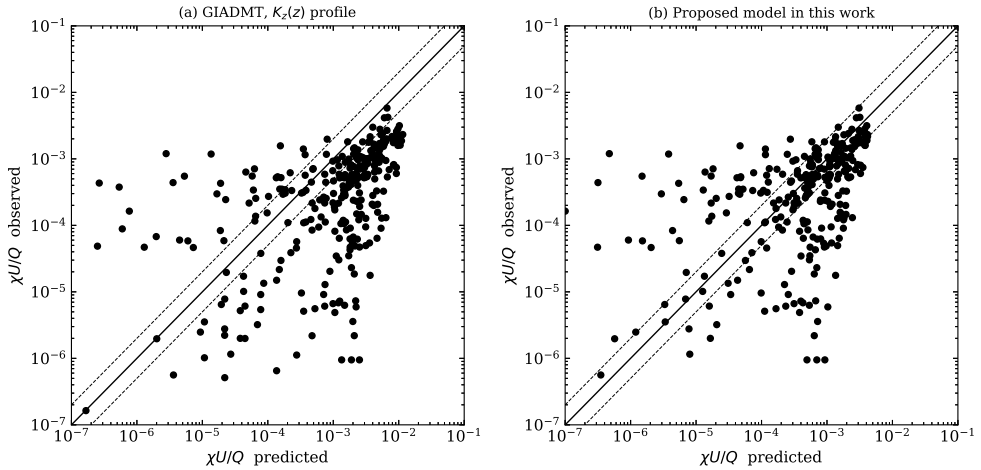


Fig. 4 INEL arcs ($N = 339$): $\chi U/Q$ predicted vs observed. (a) GIADMT with the height-dependent $K_z(z)$ profile; (b) model proposed in this work with constant K_z. Solid line $C_o = C_p$; dashed lines, FA2 band.

5 Conclusions

In this work, an analytical model for the dispersion of contaminants in low-wind-speed conditions was developed. The model combines two elements that are treated separately and analytically: the exact closed-form solution of the three-dimensional steady advection–diffusion equation with constant but distinct eddy diffusivities K_x, K_y and

K_z (Eq. (5)), which retains the longitudinal diffusion term that cannot be neglected at the small Péclet numbers typical of weak winds, and an angular convolution of this plume over a Gaussian distribution of wind directions (Eq. (7)), which represents the meandering of the horizontal wind explicitly rather than absorbing it into an enhanced lateral diffusivity. The horizontal eddy diffusivities were derived from Taylor's statistical diffusion theory applied to the low-wind velocity spectrum of Mortarini and Anfossi [27], which contains the meandering peak described by the Frenkiel autocorrelation function (Eq. (10)), while the vertical eddy diffusivity was parameterised according to the stability regime (Eqs. (11) and (12)). The angular width of the meandering was obtained from the lateral velocity standard deviation, $\sigma_\theta = \sigma_v/U$, with the low-wind floor $\sigma_v \geq 0.5\,\mathrm{m\,s^{-1}}$ suggested by the observations [1, 17].

The results obtained with the model proposed in this work are satisfactory when compared with the experimental data of the INEL experiment in a stable regime and the IIT Delhi experiment in a convective regime, as indicated in Tables 3 and 5 and Figs. 1 and 2: all the statistical indices satisfy the usual acceptance criteria, with factor-of-two fractions of 0.87 and 0.88, respectively. A more demanding test, the angular distribution of the concentration along the INEL sampling arcs, showed that the model reduces the root-mean-square error of the multilayer GIADMT solution, fed with the same meandering distribution, by a mean factor of about 3, uniformly across the experiments.

Furthermore, the comparison with the semi-analytical multilayer GIADMT solution [5], fed with the same horizontal eddy diffusivities and the same meandering distribution but retaining the height-dependent vertical eddy diffusivity profile, leads to an instructive conclusion: the mathematically more complex model does not improve on the constant-coefficient closed form, either for the ground-level peak or for the angular distribution along the arcs. In low-wind conditions the lateral spread is dominated by the meandering, which is captured by the angular convolution in both models, and the ground-level concentration is controlled by the value of the vertical eddy diffusivity in the thin layer between source and receptor: the height-dependent profile, which vanishes at the ground, supplies this layer with too little vertical diffusivity, suppressing the vertical dilution and inflating the predicted ground-level concentration, whereas the value evaluated at the height of the plume centreline remains well calibrated. This demonstrates that, provided the meandering and the anisotropy of the diffusion are correctly parameterised, a simple exact solution describes the dispersion in low wind at least as well as considerably more sophisticated schemes.

In future work, we intend to apply the model proposed in this work to other low-wind tracer experiments, to introduce the experiment-to-experiment variability of the mesoscale lateral variance σ_v [21, 40] in the determination of the angular width, and to combine the present angular convolution with the fractional dispersion models developed by Goulart et al. [12], which consider the anomalous nature of the geophysical turbulent flow.

Acknowledgements. This work was supported in part by CNPq and CAPES, Brazilian funding agencies.

Declarations

- Funding
  This work was supported in part by CNPq and CAPES, Brazilian funding agencies.
- Conflict of interest/Competing interests
  The authors have no competing interests to declare that are relevant to the content of this article.
- Ethics approval and consent to participate
  Not applicable
- Consent for publication
  Not applicable
- Data availability
  The experimental data used in this work were obtained from scientific articles already published and available.
- Materials availability
  Not applicable
- Code availability
  The computer codes used to generate the results are available from the corresponding author upon reasonable request.
- Author contribution
  All authors contributed equally to this work.

References

[1] D. Anfossi, D. Oettl, G. Degrazia, A. Goulart, An analysis of sonic anemometer observations in low wind speed conditions, Boundary-Layer Meteorol., 114 (2005) 179–203.

[2] J.C. Carvalho, G.A. Degrazia, M.T. Vilhena, S.G. Magalhães, A.G. Goulart, D. Anfossi, O.C. Acevedo, O.L.L. Moraes, Parameterization of meandering phenomenon in a stable atmospheric boundary layer, Physica A, 368 (2006) 247–256.

[3] J.C. Carvalho, M.T.M.B. Vilhena, M. Thomson, An iterative Langevin solution for turbulent dispersion in the atmosphere, J. Comput. Appl. Math., 206 (2007) 534–548.

[4] M.C. Cirillo, A.A. Poli, An intercomparison of semiempirical diffusion models under low wind speed, stable conditions, Atmos. Environ., 26A(5) (1992) 765–774.

[5] C.P. Costa, M.T. Vilhena, D.M. Moreira, T. Tirabassi, Semi-analytical solution of the steady three-dimensional advection–diffusion equation in the planetary boundary layer, Atmos. Environ., 40 (2006) 5659–5669.

[6] G.A. Degrazia, O.L.L. Moraes, A model for eddy diffusivity in a stable boundary layer, Boundary-Layer Meteorol., 58 (1992) 205–214.

[7] G.A. Degrazia, U. Rizza, C. Mangia, T. Tirabassi, Validation of a new turbulent parameterization for dispersion models in convective conditions, Boundary-Layer Meteorol., 85 (1997) 243–254.

[8] G.A. Degrazia, D. Anfossi, J.C. Carvalho, C. Mangia, T. Tirabassi, H.F. Campos Velho, Turbulence parameterisation for PBL dispersion models in all stability conditions, Atmos. Environ., 34 (2000) 3575–3583.

[9] G.A. Degrazia, D.M. Moreira, M.T. Vilhena, Derivation of an eddy diffusivity depending on source distance for vertically inhomogeneous turbulence in a convective boundary layer, J. Appl. Meteorol., 40 (2001) 1233–1240.

[10] F.N. Frenkiel, Turbulent diffusion: mean concentration distribution in a flow field of homogeneous turbulence, Adv. Appl. Mech., 3 (1953) 61–107.

[11] A.G.O. Goulart, G.A. Degrazia, O.C. Acevedo, D. Anfossi, Theoretical considerations of meandering winds in simplified conditions, Boundary-Layer Meteorol., 125 (2007) 279–287.

[12] A. Goulart, J.M.S. Suarez, M.J. Lazo, J.C. Marques, Evaluation of the eddy diffusivity in a pollutant dispersion model in the planetary boundary layer, Environ. Fluid Mech., 24 (2024) 489–504.

[13] T. Hall, G. Spindler, P. Becker, K. Grünewald, C. Pargmann, F. Duschek, Propagation of low-quality laser beams in turbulent air: new fast simulation methods and experimental results, Appl. Phys. B, 123 (2017) 271.

[14] N. Hamilton, P. Doubrawa, P. Moriarty, S. Letizia, R. Thedin, Modal dynamics of wind turbine wake meandering from lidar observations, Renew. Energy, 254 (2025) 123555.

[15] S.R. Hanna, Applications in air pollution modeling, in: F.T.M. Nieuwstadt, H. van Dop (Eds.), Atmospheric Turbulence and Air Pollution Modelling, Reidel, Dordrecht, 1982, pp. 275–310.

[16] S.R. Hanna, Confidence limits for air quality model evaluations, as estimated by bootstrap and jackknife resampling methods, Atmos. Environ., 23(6) (1989) 1385–1398.

[17] S.R. Hanna, Lateral dispersion in light-wind stable conditions, Il Nuovo Cimento, 13C (1990) 889–894.

[18] I.I. Hirschman, D.V. Widder, The Convolution Transform, Princeton University Press, Princeton, 1955.

[19] J.S. Irwin, A theoretical variation of the wind profile power-law exponent as a function of surface roughness and stability, Atmos. Environ., 13 (1979) 191–194.

[20] A.K. Luhar, M.F. Hibberd, M.S. Borgas, A skewed meandering plume model for concentration statistics in the convective boundary layer, Atmos. Environ., 34 (2000) 3599–3616.

[21] L. Mahrt, Weak-wind mesoscale meandering in the nocturnal boundary layer, Environ. Fluid Mech., 7 (2007) 331–347.

[22] R.H. Maryon, Determining cross-wind variance for low frequency wind meander, Atmos. Environ., 32 (1998) 115–121.

[23] L.P. Moor, G.A. Degrazia, M.B. Stefanello, L. Mortarini, O.C. Acevedo, S. Maldaner, C.R.P. Szinvelski, D.R. Roberti, L. Buligon, D. Anfossi, Proposal of a new autocorrelation function in low wind speed conditions, Physica A, 438 (2015) 286–292.

[24] D.M. Moreira, T. Tirabassi, J.C. Carvalho, Plume dispersion simulation in low wind conditions in stable and convective boundary layers, Atmos. Environ., 39 (2005) 3643–3650.

[25] L. Mortarini, E. Ferrero, R. Richiardone, S. Falabino, D. Anfossi, S. Trini Castelli, E. Carretto, Assessment of dispersion parameterizations through wind data measured by three sonic anemometers in an urban canopy, Adv. Sci. Res., 3 (2009) 91–98.

[26] L. Mortarini, E. Ferrero, S. Falabino, S. Trini Castelli, R. Richiardone, D. Anfossi, Low-frequency processes and turbulence structure in a perturbed boundary layer, Q. J. R. Meteorol. Soc., 139 (2013) 1059–1072.

[27] L. Mortarini, D. Anfossi, Proposal of an empirical velocity spectrum formula in low-wind speed conditions, Q. J. R. Meteorol. Soc., 141 (2015) 85–97.

[28] D. Oettl, A. Goulart, G. Degrazia, D. Anfossi, A new hypothesis on meandering atmospheric flows in low wind speed conditions, Atmos. Environ., 39 (2005) 1739–1748.

[29] M. Pahlow, M.B. Parlange, F. Porté-Agel, On Monin–Obukhov similarity in the stable atmospheric boundary layer, Boundary-Layer Meteorol., 99 (2001) 225–248.

[30] H.A. Panofsky, H. Tennekes, D.H. Lenschow, J.C. Wyngaard, The characteristics of turbulent velocity components in the surface layer under convective conditions, Boundary-Layer Meteorol., 11 (1977) 355–361.

[31] H.A. Panofsky, J.A. Dutton, Atmospheric Turbulence: Models and Methods for Engineering Applications, John Wiley & Sons, New York, 1984.

[32] J.F. Sagendorf, C.R. Dickson, Diffusion under low wind-speed, inversion conditions, NOAA Technical Memorandum ERL ARL-52, 1974.

[33] B.L. Sawford, H. Stapountzis, Concentration fluctuations according to fluctuating plume models in one and two dimensions, Boundary-Layer Meteorol., 37 (1986) 89–105.

[34] M. Sharan, M.P. Singh, A.K. Yadav, Mathematical model for atmospheric dispersion in low winds with eddy diffusivities as linear functions of downwind distance, Atmos. Environ., 30 (1996) 1137–1145.

[35] M. Sharan, A.K. Yadav, M.P. Singh, P. Agarwal, S. Nigam, A mathematical model for the dispersion of air pollutants in low wind conditions, Atmos. Environ., 30 (1996) 1209–1220.

[36] M. Sharan, A.K. Yadav, M. Modani, Simulation of short-range diffusion experiment in low-wind convective conditions, Atmos. Environ., 36 (2002) 1901–1906.

[37] M.B. Stefanello, G.A. Degrazia, L. Mortarini, L. Buligon, S. Maldaner, J.C. Carvalho, O.C. Acevedo, L.G.N. Martins, D. Anfossi, C. Buriol, D. Roberti, Development of an analytical Lagrangian model for passive scalar dispersion in low-wind speed meandering conditions, Physica A, 492 (2018) 1007–1015.

[38] W. Ulmer, Convolution/deconvolution of generalized Gaussian kernels with applications to proton/photon physics and electron capture of charged particles, in: Conference on Mathematical Models in Physics, Budapest, 2012.

[39] A. Venkatram, V. Isakov, J. Yuan, D. Pankratz, Modeling dispersion at distances of meters from urban sources, Atmos. Environ., 38 (2004) 4633–4641.

[40] D. Vickers, L. Mahrt, Observations of the cross-wind velocity variance in the stable boundary layer, Environ. Fluid Mech., 7 (2007) 55–71.

[41] E. Yee, D.J. Wilson, A comparison of the detailed structure in dispersing tracer plumes measured in grid-generated turbulence with a meandering plume model incorporating internal fluctuations, Boundary-Layer Meteorol., 94 (2000) 253–296.